Journal of
Ceramic Science
and Technology

J. Ceram. Sci. Tech., **04** [04] 177-186 (2013)
DOI: 10.4416/JCST2013-00014
available online at: http://www.ceramic-science.com

Effect of *In Situ*-Formed Cerium Hexaaluminate Precipitates on Properties of Alumina -24 Vol% Zirconia (1.4Y) Composites

F. Kern*

University of Stuttgart, IFKB, Allmandring 7B, D-70569 Stuttgart, Germany
received May 14, 2013; received in revised form June 18, 2013; accepted August 5, 2013

Abstract

***In situ*-platelet-reinforced zirconia-toughened alumina ceramics have become established materials, successfully replacing alumina and zirconia in hip implants. While the beneficial effect of the *in situ* toughening seems undoubted, this toughening mechanism is still not fully understood.**

A nanocomposite ZTA containing 24 vol% partially stabilized zirconia (1.4Y-TZP) was reinforced with 10 vol% cerium hexaaluminate (CA6) by reacting *in situ*-reduced ceria with alumina during hot pressing. The mechanical properties, evolution of microstructure and phase composition of the CA6-containing ZTA were compared with the properties of the non-reinforced reference.

The unreinforced ZTA24 shows a microstructure with modular matrix grains and ultrafine zirconia dispersion. High strength of 1150 MPa but moderate toughness of 5 MPa·√m and low transformability of the zirconia dispersion was observed. The CA6-reinforced material shows higher toughness and transformability combined with a trade-off in hardness and strength. The CA6 precipitates are rod-shaped, well dispersed and oriented normal to the pressing direction. The formation of CA6 especially at sintering temperatures exceeding 1500 °C is associated with microstructural coarsening and a broadening of grain size distribution of matrix and dispersion, making the zirconia more transformable. Crack deflection at matrix-precipitate grain boundaries was not observed.

Keywords: Alumina, zirconia, platelets, mechanical properties, microstructure

I. Introduction

Zirconia-toughened alumina materials were designed to preserve the high hardness and abrasion resistance of alumina while achieving improved fracture toughness and strength with addition of the zirconia dispersion [1]. Although the individual reinforcement mechanisms in ZTA are well documented, their interaction seems very complex. It is quoted that transformation toughening by martensitic phase transformation of small metastable tetragonal grains increases both strength and toughness [2]. Microcracking by existing microcracks which are formed by transformation of large zirconia grains during cooling improves toughness but is detrimental to strength [3]. The contribution of microcracking during fracture induced by phase transformation or residual stress was discussed but is difficult to quantify [1]. Residual stress induced by thermal mismatch of alumina and zirconia as such can act as to increase the fracture resistance in the matrix, provided that the monoclinic content of zirconia in as-fired state is kept below a threshold value of ~ 20 vol% (stress neutrality) [4].

Platelet reinforcement can be achieved by adding alumina platelets, such materials are, however, difficult to densify by means of pressureless sintering owing to the high aspect ratio of the reinforcing structures [5]. *In situ* platelet reinforcement by strontium hexaaluminate formation was first applied to Ce-TZP by Cutler with the effect that fracture toughness was improved compared with the alumina-toughened material [6]. Burger applied the concept to ZTA [7]. The platelet-reinforced ZTA has become the reference material in hip and knee arthroplasty owing to its high strength hardness and toughness combined with high aging resistance [8].

Besides the type $MAl_{12}O_{19}$ (M = Sr, Ba), the type $MAl_{11}O_{18}$ (M = La, Nd, Ce) was tried for reinforcement of ZTA [7, 9, 10]. The metal cations M are either added as oxides or released from ternary compounds such as $SrZrO_3$.

In hot-pressed or SPS-sintered ceramics, cerium hexaaluminate (CA6) platelets can be formed by *in situ* reduction of dispersed Ce(IV)-oxide with carbon or carbon monoxide traces from the graphite mould and reaction with excess alumina.

Ceria(IV) reduction is favoured by low partial pressures and high temperatures [11]. Tsukuma produced Y-TZP reinforced with 40 vol % CA6-platelets and proved the reversibility of the reduction process [12]. The first quote on SPS-sintered CA6-reinforced ZTA by Akin shows a reduction of toughness with CA6 addition and no crack deflection at platelet interfaces [13]. However, the materials studied by Akin were made with untransformable 3Y-TZP. A study by the author shows that in ZTA reinforced with 10 vol% unstabilized zirconia and 5 vol% CA6, an increase of fracture toughness can be observed [14]. High sintering temperatures favour – along with the expected

* Corresponding author: frank.kern@ifkb.uni-stuttgart.de

formation of CA6 – the formation of large alumina grains containing intragranular zirconia. Crack deflection was observed not along CA6 boundaries but along boundaries of large alumina grains.

The present study aims at clarifying the effect of CA6 on mechanical behaviour in ZTA materials containing zirconia contents above the percolation level and the feasibility to use the material system for high-performance ceramics requiring sintering in non-oxidizing atmosphere.

II. Experimental

The feedstocks were prepared with a mixing and milling approach. The raw materials used were alumina APA0.5 (Ceralox, USA, S_{BET} = 8 m²/g, d_{50} = 300 nm), unstabilized zirconia UEP (DKKK, Japan, S_{BET} = 23 m²/g), cerium dioxide (Chempur, Germany, purity 99.9 %, d_{50} = 5 μm) and yttrium oxide (Aldrich, Germany, purity 99,9 %). 200 g of the powder mixtures were dispersed in 250 ml 2-propanol and milled for 24 h at 300 rpm in an attritor with Y-TZP balls (d = 0.8 – 1 mm). The prolonged milling time was required to ensure good dispersion of yttria and comminution of ceria. Based on previous studies by Sommer the zirconia content was set at 24 vol%, the stabilizer content of the zirconia set at 1.4 mol% [15]. In the ceria-containing feedstock ZTA24-Ce, 2.4 mass% of the alumina were replaced with cerium dioxide. Assuming complete reaction to aluminate this composition should provide ~ 10 vol% of CA6 precipitates (the exact density of CA6 is unknown). Milling media were then separated and the feedstock was dried at 85 °C overnight and screened through a 125 μm mesh.

Two samples (d = 45 mm, h = 2 mm) of each parameter set were hot pressed at a heating rate of 50 K/min at 1425 °C – 1550 °C in vacuum at 40 MPa axial pressure and 2 h dwell (KCE, Germany). The pressed specimens were subsequently lapped with 15-μm diamond suspension and polished with 15 μm, 6 μm and 1 μm diamond suspension (Struers, Denmark). The samples were then cut into bars of 4 mm in width. The Vickers hardness HV10 (Bareiss, Germany, five indents) and HV0.1 (Fischer, Germany, 12 indents) were measured, the indentation modulus E_{IND} was determined from the loading-unloading curve of the microhardness measurement. The bending strength σ_{4pt} was determined by a 4-point measurement with 20 mm outer and 10 mm inner span at a crosshead speed of 0.5 mm/min (Zwick, Germany). The fracture resistance K_{ISB} was determined by indentation strength in bending [16]. Three bars were indented with a HV10 indent on the tensile side and the residual strength was measured in the same 4-pt setup at a crosshead speed of 1.5 mm/min immediately after indentation to suppress subcritical crack growth. Resistance to subcritical crack growth was determined by stable indentation crack growth in bending on bars pre-notched with four HV10 indents on the tensile side at a crosshead speed of 2.5 mm/min. The pre-indented bars were stored for two weeks in ambient air to allow the cracks to grow to a stable extension, the initial load was chosen as one third of the residual strength determined in the ISB test (~ 70 MPa). This method was proposed by Braun and refined by Dransmann and Benzaid [17–19]. The method has been applied and its limits discussed elsewhere [20].

The phase composition of the polished surface and fracture face of ZTA samples was determined with XRD (Bruker D8, Germany, CuKα, graphite monochromator) by integrating the areas of the monoclinic (-111) and (111) reflexes and the tetragonal (101) reflex. The volumetric content of monoclinic was then calculated using the calibration curve of Toraya [21]. With the monoclinic contents the transformation zone depth h was calculated according to Kosmac, and the transformation toughness increment was calculated according to McMeeking [22, 23].

The microstructure of polished and thermally etched (1300 °C/15 min, hydrogen) surfaces was studied by means of SEM (Zeiss, Germany, secondary electrons, inlens mode, 3 kV). The grain sizes were determined with the linear intercept method [24].

III. Results

(1) Microstructure

SEM images of the microstructure of ZTA24 and ZTA24-Ce sintered at 1450 °C, 1500 °C and 1550 °C are shown in Figs. 1 and 2. Fig. 3 shows the grain sizes of alumina and zirconia in the two materials. Microstructures are pore-free and thus completely dense. In ZTA24 the majority of the alumina grains are modular. As the zirconia content is above the percolation threshold, the dispersion forms a partially connected network. Zirconia grains are almost exclusively located in intergranular position. Alumina grain sizes increase almost linearly with sintering temperature from 480 nm at 1425 °C to 900 nm at 1550 °C. The grains of the zirconia dispersion are very fine, in the applied sintering temperature range their size increases only moderately from 200 nm to 300 nm. Thus the grain size is far below the critical size for transformation. In case of ZTA24-Ce the grain sizes stay invariant at 680 nm for alumina and 200 nm for zirconia between 1425 °C and 1475 °C. At 1475 °C first grain growth in alumina starts, then between 1500 °C and 1525 °C significant grain growth of zirconia to a size of approximately 500 nm can be observed. In general the size distribution is broader in case of the ceria-containing material. The CA6 precipitates are rather rods than platelets, their size varying between 8 – 12 μm in length and 1 – 2 μm in width. Almost all precipitates are oriented normal to the pressing direction, which is an indication that the precipitate formation proceeds not during heating but during the dwell time under the influence of axial pressure. The CA6 rods have relatively flat boundaries. Zirconia grains are located generally in intergranular position, intragranular zirconia can only be found inside the CA6 rods. The zirconia content inside the rods seems lower than in the matrix, which indicates that a part of the zirconia is expelled during precipitate formation, while a certain fraction seems to be trapped owing to the fast heating rate. CA6 rods are surrounded by a verge enriched in zirconia.

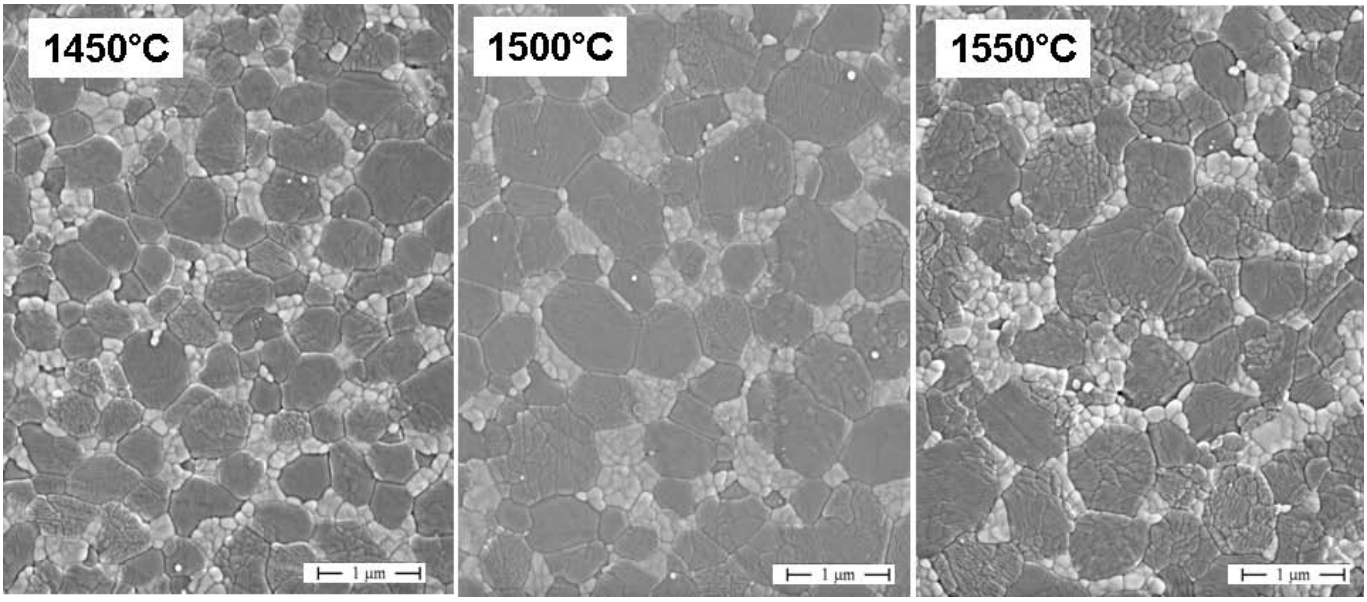

Fig. 1 : Microstructure of ZTA24 sintered at 1450 °C, 1500 °C and 1550 °C/1 h (SEM image of polished and thermally etched surface).

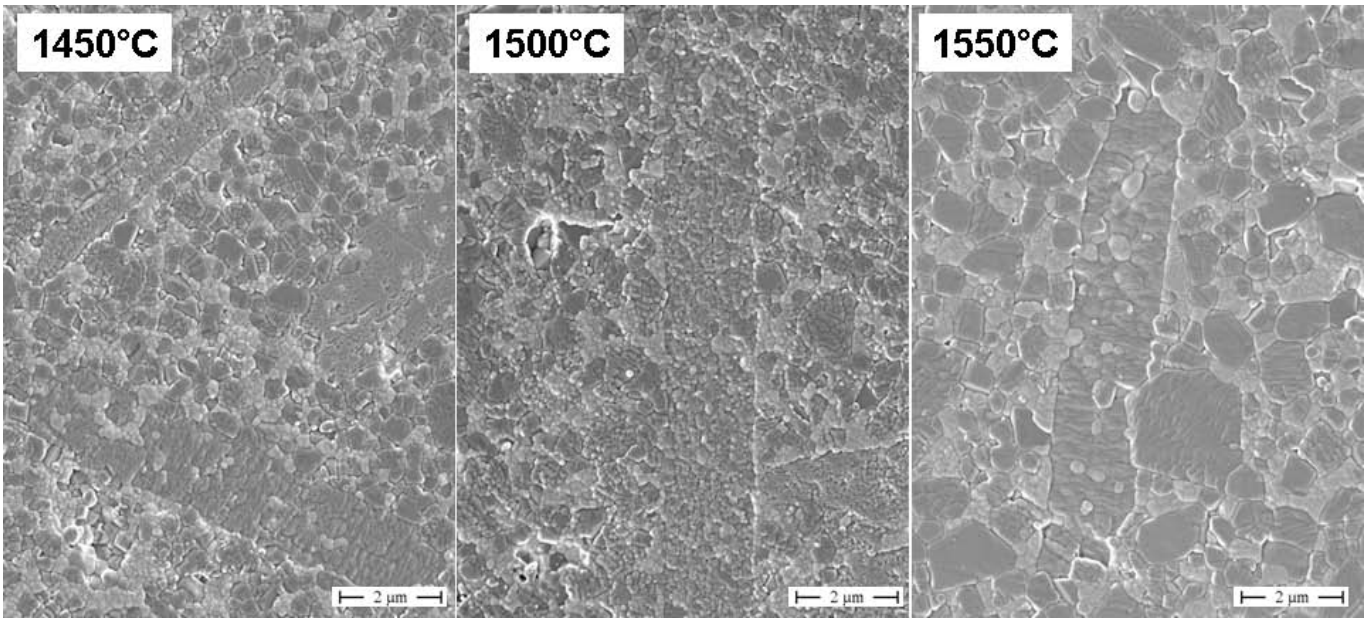

Fig. 2 : Microstructure of ZTA24-Ce sintered at 1450 °C, 1500 °C and 1550 °C/1 h (SEM image of polished and thermally etched surface).

(2) Mechanical properties

The Vickers hardness HV10 and indentation modulus of ZTA24 and ZTA24-Ce are shown in Figs. 4 and 5. Between sintering temperatures of 1425 °C and 1475 °C, hardness of ZTA24 falls linearly from 1910 to 1860 and stays at this level with increasing sintering temperature. In case of ZTA24-Ce the hardness level is generally lower by ~ 1 – 1.5 GPa, HV10 declines from 1775 at a sintering temperature of 1425 °C to 1720 at 1550 °C. The indentation modulus is quite similar for both materials between sintering temperatures of 1425 – 1525 °C. A value of ~ 360 GPa can be expected from the rule of mixture. Only at the highest temperature the modulus of ZTA24-Ce drops from 360 GPa to 330 GPa.

Fig. 6 displays the 4-pt bending strength of the two ZTA materials. ZTA24 exhibits very high strength over the whole sintering temperature range, the minimum value of 1030 MPa is obtained at 1500 °C, at all other sintering temperatures the bending strength exceeds 1100 MPa. Strength of ZTA-Ce is generally lower, the overall strength level is still attractive. The CA6-reinforced material shows a strength maximum of 1010 MPa at 1500 °C, at higher sintering temperatures the strength declines to ~ 800 MPa. The fracture resistance K_{ISB} is shown in Fig. 7. As can be expected from the rising zirconia grain sizes, both materials show a trend to increasing toughness with increasing sintering temperature. The toughness of ZTA24 is, however, always slightly lower and tends to level off at 1500 °C at a moderate value of 5 MPa·√m. The fracture resistance of ZTA24-Ce continues to rise with

sintering temperature and reaches a maximum value of 5.5 MPa·√m at 1550 °C. Interestingly the strength toughness correlation turns inverse for ZTA24-Ce. As we may assume identical initial flaw sizes, this may hint at a mechanistic change or at subcritical crack growth in the samples sintered at high temperatures having a coarser microstructure. Tests of resistance to subcritical crack growth were performed by stable indentation crack growth in flexure (Figs. 8 and 9). In case of the ZTA24, the results confirm the data measured by ISB, which *a priori* is not surprising as it is basically the same test configuration. The extrapolated $K_{IC,ext}$ values reach levels of 5.5 MPa·√m and are only slightly higher than K_{ISB}. In the case of ZTA24-Ce the results do not match. Extrapolated K_{IC} levels are significantly higher and may reach levels above 8 – 9 MPa ·√m. The small specimen size does not, however, allow for measuring in the long crack range. As Lube and Fett have shown for silicon nitride that overestimated toughness values may be obtained by nonlinearity of the residual stress coefficient χ in the long crack region, the extrapolated result therefore has to be regarded with extreme caution [25]. A more detailed look shows, however, that the stress coefficient χ (the slope of the linear section) is significantly higher in case of ZTA24-Ce, which means that the toughness rises faster with increasing crack length (Fig. 10). The location of the kink in the curve indicates the point ($K_{app,0}$) where the residual stress intensity and applied stress intensity turn equal. The resistance to subcritical crack growth K_{I0} can be determined by $K_{I0} = K_{IC} - K_{app,0}$. Fig. 8 shows the results of the experiments comparing a conservative approach in which it is assumed that $K_{IC} = K_{ISB}$. Fig. 9 presents a more optimistic approach in which the extrapolated level of $K_{IC} = K_{IC,ext}$ is used. Fig. 8 shows that in case of ZTA24, K_{I0} is in a range between 3 – 4 MPa·√m which is in accordance with existing data on ZTA determined by Gutknecht and Chevalier [26]. For ZTA24-Ce, K_{I0} is approximately 0.5 MPa·√m higher in case of the conservative approach. The optimistic approach (Fig. 9) leads to slightly elevated but still consistent K_{I0} values for ZTA24. Very high K_{I0} values in the range of 5 – 7 MPa·√m are obtained for ZTA24-Ce which seem hardly credible. In any case further studies are required to clarify this point. The cracks induced during stable indentation crack growth in flexure in a ZTA24-Ce sintered at 1500 °C are shown in Fig. 11. Within the ZTA matrix the crack runs intergranularly along alumina grain boundaries. Irrespective of the position along the crack propagation direction, no crack deflection was observed at matrix-CA6 precipitate interfaces. Even close to the crack tip, where the crack has lost most of its energy, the cracks propagate across the hexaaluminate without being deflected, cracks hitting the ends of precipitates even break lengthwise through the CA6 rods (Fig. 11c).

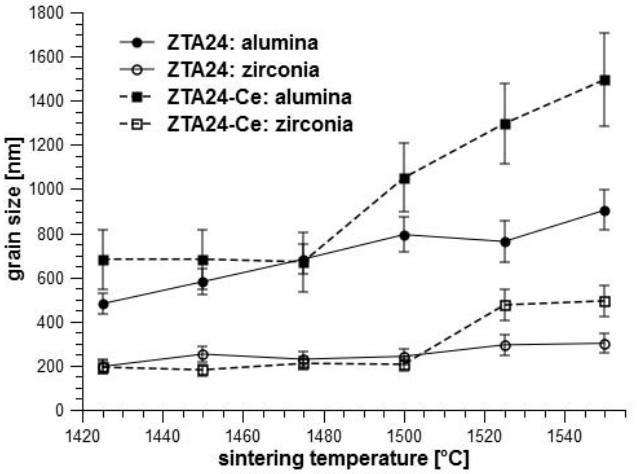

Fig. 3: Grain sizes determined with linear intercept method of alumina and zirconia in ZTA24 and ZTA24-Ce sintered at 1425 – 1550 °C.

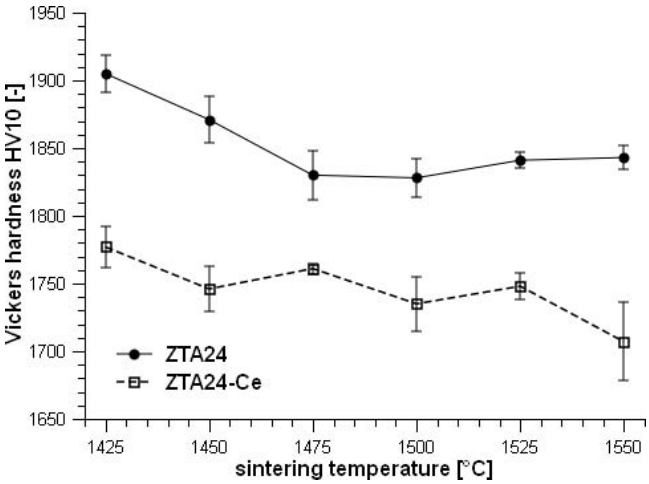

Fig. 4: Vickers hardness HV10 of ZTA24 and ZTA24-Ce sintered at 1425 – 1550 °C.

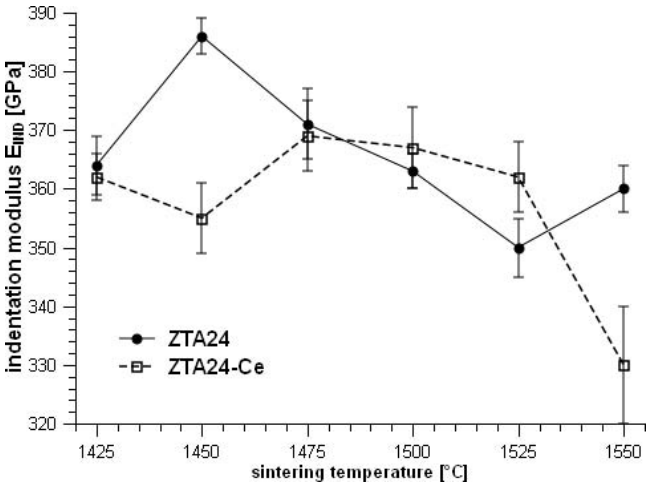

Fig. 5: Indentation modulus E_{IND} of ZTA24 and ZTA24-Ce sintered at 1425 – 1550 °C.

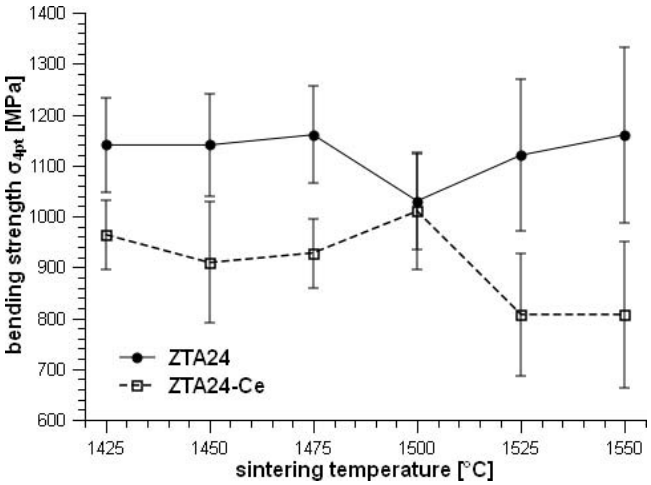

Fig. 6: Bending strength σ_{4pt} of ZTA24 and ZTA24-Ce sintered at 1425 – 1550 °C.

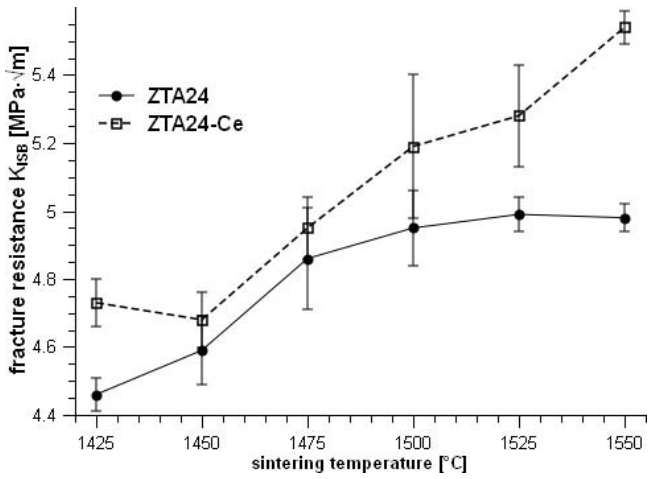

Fig. 7: Fracture resistance K_{ISB} of ZTA24 and ZTA24-Ce sintered at 1425 – 1550 °C.

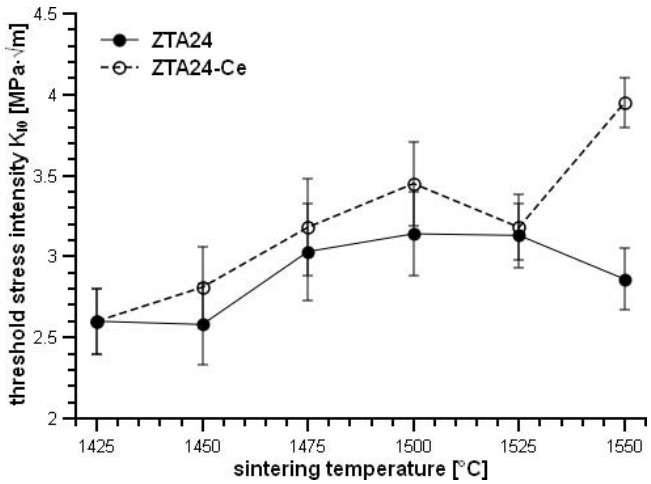

Fig. 8: Threshold stress intensity K_{I0} of ZTA24 and ZTA24-Ce sintered at 1425 – 1550 °C determined by conservative approach ($K_{I0} = K_{ISB} - K_{app,0}$).

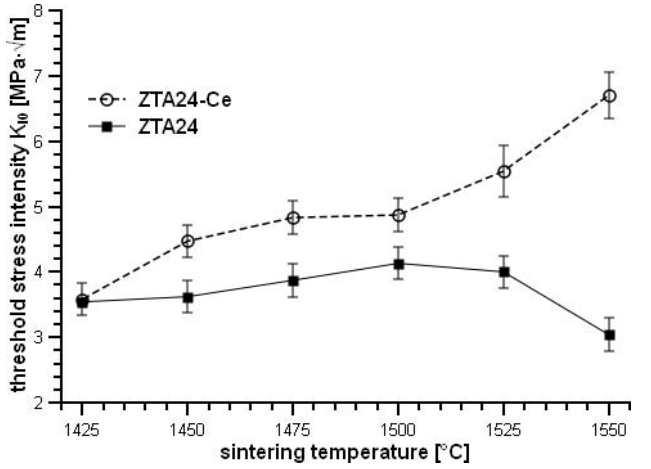

Fig. 9: Threshold stress intensity K_{I0} of ZTA24 and ZTA24-Ce sintered at 1425 – 1550 °C determined by extrapolation ($K_{I0} = K_{IC,ext} - K_{app,0}$).

Crack stopping and re-initiation, crack branching or crack deflection effects observed are not hexaaluminate-specific. Evaluation of a larger number of samples showed that these effects predominantly occur when the crack interacts with large alumina grains.

(3) Phase composition

Monoclinic contents in polished surfaces $V_{m,pol}$ and fracture faces $V_{m,FF}$ (samples from ISB test broken perfectly straight) were determined with XRD (Fig. 12). In case of ZTA24 the monoclinic contents in as-fired state are low (3 ± 1 vol%) at all sintering temperatures. In ZTA24-Ce the monoclinic contents are also low but show a clear tendency to rise with sintering temperature. As Gregori has shown, the stress neutral state is in the range of ~ 20 vol% monoclinic [4]. Thus in both materials the alumina matrix is under compressive stress, the zirconia dispersion is under tension which should favour transformation.

However, the monoclinic content in the fracture faces of ZTA24 is also very low, a maximum value of 12 ± 3 vol% was measured at a sintering temperature of 1450 °C, all other samples had less than 10 vol% monoclinic. The dispersion can thus be considered almost untransformable independent of the applied sintering temperature.

The monoclinic contents in the fracture faces of ZTA24-Ce start to rise at sintering temperatures > 1475 °C. In the temperature range between 1500 °C – 1550 °C the resulting transformability $V_f = V_{m,FF} - V_{m,pol}$ reaches a level of 20 %, which is three times the maximum value observed on ZTA24.

With the measured values of $V_{m,FF}$ and $V_{m,pol}$ the transformation zone height h can be calculated using the formula of Kosmac [22]. The McMeeking formula can be applied to calculate the transformation toughness increment ΔK_{IC}^T [23]. In Fig. 13 the calculated values of h and ΔK_{IC}^T are shown. The transformation zones in ZTA24 are very small (h < 1 μm) irrespective of sintering temperature. In ZTA24-Ce larger transformation zones (h > 2 μm) are formed at sintering temperatures higher than 1500 °C. The resulting transformation toughness increments (ΔK_{IC}^T ~ 0.1 MPa·√m) are almost negligible for ZTA24. In case of ZTA24-Ce moderate transformation toughness increments of ΔK_{IC}^T ~ 0.35 – 0.45 MPa·√m are

calculated for materials sintered at 1500 – 1550 °C. The difference in $\Delta K_{IC}{}^{T}$ values for ZTA24 and ZTA24-Ce corresponds very well to the difference in measured K_{ISB} toughness values.

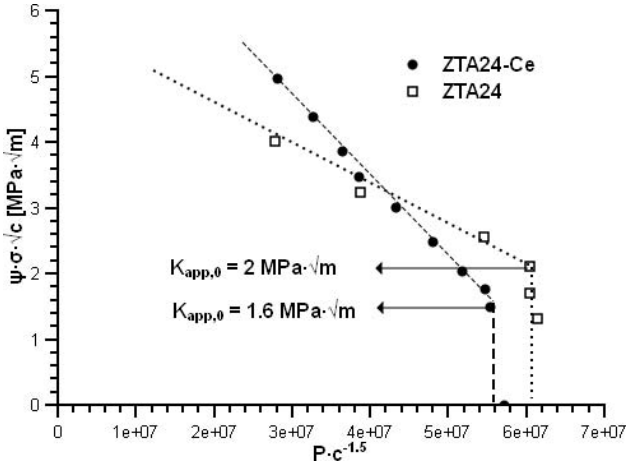

Fig. 10: Stable indentation crack growth in flexure, plot of measured data for ZTA24 and ZTA24-Ce sintered at 1550 °C.

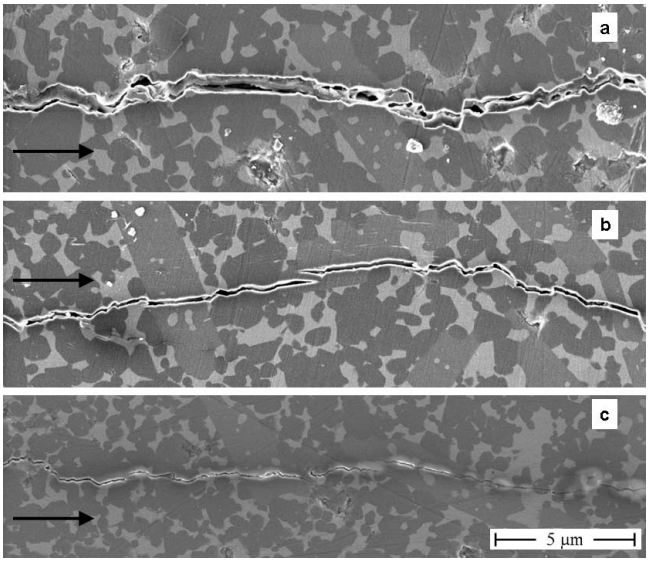

Fig. 11: Crack path through ZTA24-Ce sintered at 1500 °C (SEM image of non-etched surface, arrows indicate the direction of crack progression); a: near crack origin/indent; b: middle region; c: near crack tip.

Fig. 14 shows the fingerprint area of the XRD patterns of the ZTA-CA6 at 32 – 37° 2θ-scale containing the most intensive reflexes (110) of $CeAlO_3$ (JCPDS 28 – 0260) at 33.6° 2θ and (107) of $CeAl_{11}O_{18}$ (JCPDS 48 – 0055) at 34.2° 2θ. While the material sintered at 1450 °C shows only the reflexes of CA6, the material sintered at the lowest temperature clearly shows the presence of $CeAlO_3$ in a relevant quantity. A rough quantification can be carried out indirectly using the area of the (002) reflex of t-ZrO_2 as an internal reference and calculating the ratio $R = A(107)_{CA6}/A(002)_{ZrO2}$. Assuming complete conversion to CA6 at 1450 °C the ratio R(1425 °C)/R(1450 °C) = $X_{CA6} = 0.7 \pm 0.13$. This means that at 1425 °C about 30 % of the trivalent ceria is still contained in the monoaluminate which may thus be interpreted as the intermediate product of a two-stage consecutive reaction to the stable hexaaluminate.

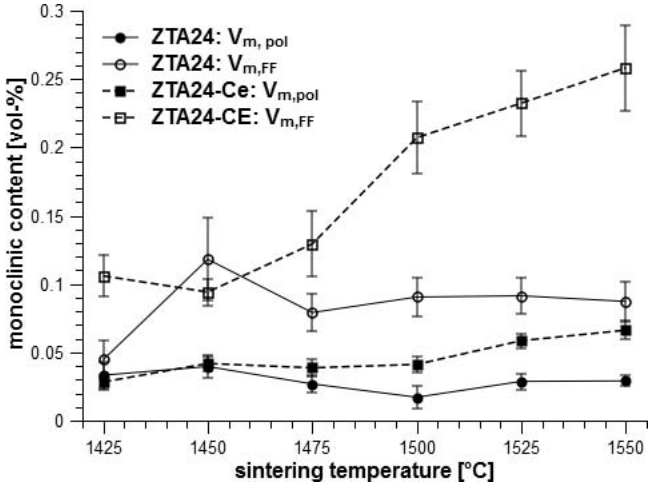

Fig. 12: Monoclinic contents determined by XRD in polished surfaces and fracture faces of ZTA24 and ZTA24-Ce sintered at 1425 – 1550 °C.

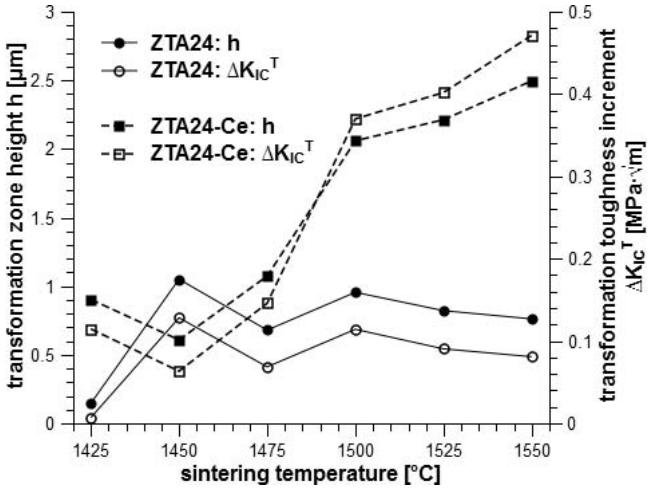

Fig. 13: Transformation zone depth h and transformation toughness increments $\Delta K_{IC}{}^{T}$ of ZTA24 and ZTA24-Ce sintered at 1425 – 1550 °C.

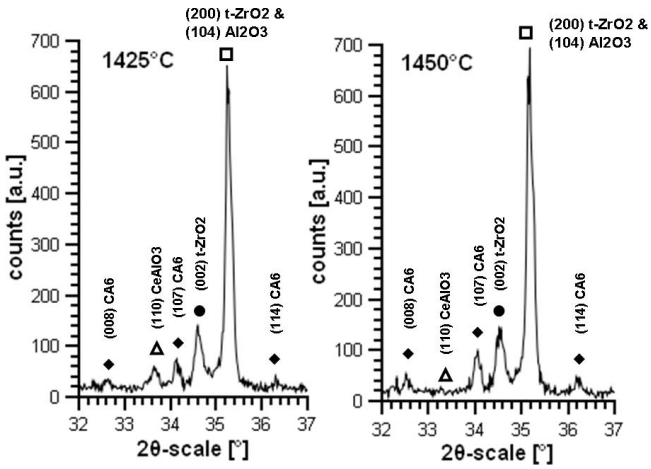

Fig. 14: Fingerprint area of the XRD patterns of ZTA-CA6 sintered at 1425 °C and 1450 °C (2θ-scale of 32 – 37°) showing the characteristic reflexes of $CeAlO_3$ and $CeAl_{11}O_{18}$.

IV. Discussion

It was found that the addition of ceria to ZTA sintered under reducing conditions leads to the formation of rod-

shaped CA6 precipitates homogeneously dispersed in the matrix. CA6 rods have length of ~ 10 μm and a width of ~ 1 – 2 μm. While the ZTA24 retains its fine-grained microstructure with modular alumina grains and small zirconia grains in intergranular position the CA6 formation is associated with a microstructural coarsening of the matrix as well as the zirconia dispersion at sintering temperatures of > 1475 °C. In the vicinity of the CA6 rods the uniform distribution of zirconia is disturbed. Zirconia grains are preferentially located on the boundaries of CA6, in the rods a depletion of zirconia can be observed. A shift to exaggerated grain growth and an inter-type structure at sintering temperatures > 1500 °C as reported in ZTA with 10 vol% zirconia was not observed, presumably the higher fraction of zirconia is able to stabilize the inter-type structure [14].

The microstructural differences are reflected in the mechanical properties and in the phase composition. Larger zirconia grains in ZTA24-Ce are more transformable, boosting the transformability, transformation zone sizes and consequently the transformation toughness increments. While ZTA24 is virtually untransformable, the transformation toughness increments in ZTA24-Ce reach values of up to 0.45 MPa·√m.

The results concerning the resistance to subcritical crack growth are consistent in case of ZTA24 but somewhat contradictory in case of ZTA24-Ce. Undoubtedly the toughness rises faster with increasing crack length in case of ZTA24-Ce. This hints at an interaction of the crack with the precipitates, which was, however, not confirmed by SEM studies of crack paths. In fact the indentation-induced cracks run straight in case of ZTA24 and are kinked in the case of ZTA24-Ce. A direct interaction of the crack with the precipitates was, however, not observed. Cracks are deflected at the grain boundaries of larger alumina grains.

The extremely fine grain and isotropic structure of ZTA24 seem to be very favourable to reach a high strength. In case of ZTA24-Ce the highest strength is reached at a sintering temperature of 1500 °C, marking the transition range between fine-grain and coarsened structures. At this temperature alumina has started coarsening while zirconia is still fine-grained. Interestingly here the transformability of zirconia rises without a measurable increase in its average grain size compared to the sample sintered at 1475 °C. It seems that the transformation of zirconia not only depends on its grain size and inter- or intragranular position alone as shown by Heuer but is also triggered by the structure of the surrounding alumina matrix [27]. Once zirconia grains start to grow, the bending strength drops by 200 MPa. The evaluation of the compiled results indicates that the toughening by the *in-situ* aluminate formation is a cooperative effect consisting of three components. Promotion of grain growth favours higher transformability and higher transformation toughness, at the same time the state of residual stress is changed, compressive stress in the matrix and tensile stress in the dispersion are reduced. Microcrack formation was not observed in as-fired samples, however during fracture with proceeding phase transformation, formation of microcracks may occur which consumes fracture energy but may reduce strength. At the same time in a microcracked material the elastic modulus may locally be reduced and only then crack deflection at precipitates can take place, improving the toughness in the long-crack regime. In the undamaged matrix, according to He and Hutchison. the crack will not be deflected at an interface between a high modulus matrix and a lower modulus reinforcement [28]. One may speculate that this explains the high extrapolated toughness values. For the practical application of the materials and the resistance to fast fracture, this effect is, however, of minor importance.

Concerning the phase formation of CA6, the existing results indicate that the phase formation is incomplete at the lowest sintering temperature of 1425 °C, but completed at 1450 °C. A complete survey of the mechanism and kinetics of the CA6 formation would exceed the scope of the present publication. Different reaction scenarios may be depicted in which the CA6 is directly formed from reduced ceria and alumina or via an intermediate formation of the monoaluminate $CeAlO_3$. So far it can be confirmed that $CeAlO_3$ as an intermediate product is formed at the lowest sintering temperature. The monoaluminate formation hints at a local supersaturation with Ceria(III) which at longer time at higher temperature is eliminated and the stable hexaaluminate is formed. However, this does not necessarily mean that direct formation of CA6 can *a priori* be excluded.

Moreover uptake into and release of ceria from solid solutions in zirconia could occur, however, considering the high heating rate they seem unlikely as they would require fast redistribution of ceria by diffusion over distances of micrometers. Literature on the subject is incomplete and limited to subsystems. According to thermodynamic calculations of Huang for 12Ce-TZP at 1500 °C the fraction of trivalent ceria increases from 27 % in air to 90 % for vacuum in a graphite furnace [11]. Data on the system alumina-zirconia-ceria(III) are unavailable. For the similar alumina-zirconia-lanthana system Lakiza and Lopato have plotted the isopleth at 20 mol% zirconia [29]. For temperatures of 1500 – 1600 °C and small lanthana contents they found a very narrow tetragonal field where some lanthana is contained as a solid solution in the zirconia besides alumina and the hexaaluminate LA6. In the lanthana-zirconia subsystem, this narrow tetragonal field of lanthana solid solution with a maximum content of 0.13 mol% lanthana is also contained, the tetragonal wedge narrows considerably at lower temperatures to disappear completely at 1100 °C [30]. Another unknown factor is the addition of yttria which stabilizes the tetragonal phase and thus possibly also the solid solution of ceria (III). Present results do not provide any clue concerning this point.

V. Conclusions

Cerium-hexaaluminate-reinforced ZTA materials were successfully produced by reaction sintering of *in situ*-reduced cerium dioxide with excess alumina. Compared to the non-reinforced reference ZTA, lower hardness and strength were observed. Improved fracture resistance of hexaaluminate-toughened material can be attributed to higher transformability of the zirconia reinforcement which is triggered by larger grain sizes compared to plain

ZTA. Fracture resistance in hexaaluminate-toughened materials increases faster with increasing crack length, which indicates a steeper R-curve. The resistance to subcritical crack growth (measured by stable indentation crack growth in flexure) is improved by platelet reinforcement. The proportion of this threshold fracture resistance improvement that can be reliably quantified amounts to $\Delta K_{IC} = 0.5 - 1\ MPa \cdot \sqrt{m}$ in samples sintered at < 1500 °C. In samples sintered at higher temperature the increase in threshold toughness maybe even higher, however, extrapolated toughness determined by this procedure may be exaggerated. Further studies will be necessary to clarify this effect. Indications for direct toughness enhancement by crack deflection at CA6 rods were not found. It thus seems that the reinforcement effect of the *in-situ*-formed cerium hexaaluminate is a cooperative effect mainly caused by a moderate coarsening of the microstructure which results in higher transformability of zirconia and a different state of residual stress. It may be speculated that crack deflection is active in the long crack range of oversintered materials having a globally or locally lower elastic modulus induced by microcracking. *In situ* reinforcement by cerium hexaaluminate is an attractive technology to improve the mechanical properties of alumina-zirconia composites that require sintering under reducing conditions such as in hot pressing or SPS. A separate study of the cerium hexaaluminate formation mechanism could be the basis to obtain materials with more sophistically tailored compositions and microstructures depending on recipes, heating and cooling conditions. Especially size, distribution and orientation of CA6 precipitates may strongly influence the mechanical properties of the composites.

References

1 Wang, J., Stevens. R.: Zirconia-toughened alumina (ZTA) ceramics, *J. Mater. Sci.*, **24**, 3421 – 3440, (1989).

2 Becher, P.F.: Slow crack growth behavior in transformation-toughened Al_2O_3-$ZrO_2(Y_2O_3)$ ceramics, *J. Am. Ceram. Soc.*, **66**, [7], 485 – 488, (1983).

3 Claussen, N.: Fracture toughness of Al_2O_3 with an unstabilized ZrO_2 dispersed phase, *J. Am. Ceram. Soc.*, **59**, [1 – 2], 49 – 51, (1976).

4 Gregori, G., Burger, W., Sergo, V.: Piezo-spectroscopic analysis of the residual stresses in zirconia-toughened alumina ceramics: the influence of the Tetragonal-to-monoclinic transformation, *Mater. Sci. Eng. A,* **271**, 401 – 406, (1999).

5 Garcia D.E., Rödel, J., Claussen, N.: Subcritical crack growth and R-curve behavior in Al_2O_3-Toughened Y-TZP, in Science and Technology of Zirconia V. Technomic Publishing, Lancaster, USA, 1993.

6 Cutler, R.A., Mayhew, R.J., Prettyman, K.M., Virkar, A.V.: High-toughness Ce-TZP/Al_2O_3 ceramics with improved hardness and strength, *J. Am. Ceram. Soc.,* **74**, [1], 179 – 86, (1991).

7 Burger, W., Richter, H.G.: High strength and toughness alumina matrix composites by transformation toughening and in situ platelet reinforcement (ZPTA) – the new generation of bioceramics, *Key Eng. Mat.*, **192 – 195**, 545 – 548, (2001).

8 Chevalier, J., Grandjean, S., Kuntz, M., Pezzotti, G.: On the kinetics and impact of tetragonal to monoclinic transformation in an alumina/zirconia composite for arthroplasty applications, *Biomaterials*, **30**, [29], 5279 – 5282, (2009).

9 Wu, Y., Zhang, Y., Huang, X., Guo, J.: In-situ growth of needle-like $LaAl_{11}O_{18}$ for reinforcement of alumina composites, *Ceram. Int.*, **27**, 903 – 906, (2001).

10 Jin, X., Gao, L.: Effects of powder preparation method on the microstructure and mechanical performance of ZTA/$LaAl_{11}O_{18}$ composites, *J. Eur. Ceram. Soc.*, **24**, 653 – 659, (2004).

11 Huang, S., Li, L., Vleugels, J., Wang, P., Van der Biest, O.: Thermodynamic prediction of the nonstoichiometric phase $Zr_{1-z}Ce_zO_{2-x}$ in the ZrO_2-$CeO_{1.5}$-CeO_2 system, *J. Eur. Ceram. Soc.*, **23**, 99 – 106, (2003).

12 Tsukuma, K.: Conversion from β-$Ce_2O_3 \cdot 11\ Al_2O_3$ to α-Al_2O_3 in tetragonal ZrO_2 matrix, *J. Am. Ceram. Soc.,* **83**, [12], 3219 – 21, (2000).

13 Akin, I., Yilmaz, E., Sahin, F., Yucel, O., Goller, G.: Effect of CeO_2 addition on densification and microstructure of Al_2O_3-YSZ composites, *Ceram. Int.,* **37**, 3273 – 3280, (2011).

14 Kern, F.: Structure-property relations in alumina-zirconia nanocomposites reinforced with in situ formed cerium hexaaluminate precipitates, *Scripta Mater.*, **67**, [12], 1007 – 1010, 2012.

15 Sommer, F., Landfried, R., Kern, F., Gadow, R.: Mechanical properties of zirconia toughened alumina with 10 – 24 vol% 1.5 mol% Y-TZP reinforcement, *J. Eur. Ceram. Soc.*, **32**, [15], 3905 – 3910, (2012).

16 Chantikul, P., Anstis, G.R., Lawn, B.R., Marshall, D.B.: A critical evaluation of indentation techniques for measuring fracture toughness: II, strength method, *J. Am. Ceram. Soc.*, **64**, [9], 539 – 543, (1981).

17 Braun, L.M., Benninson, S.J., Lawn, B.R.: Objective evaluation of short-crack toughness curves using indentation flaws: case study on alumina-based ceramics, *J. Am. Ceram. Soc.*, **75**, [11], 3049 – 57, (1992).

18 Dransmann, G., Steinbrech, R., Pajares, A., Guiberteau, F., Dominguez-Rodriguez, A., Heuer, A.: Indentation studies on Y_2O_3,-stabilized ZrO_2: II, Toughness determination from stable growth of indentation-induced cracks, *J. Am. Ceram. Soc.*, **77**, [5], 1194 – 201, (1994).

19 Benzaid, R., Chevalier, J., Saadaoui, M., Fantozzi, G., Nawa, M., Diaz, L.A., Torrecillas, R.: Fracture toughness, strength and slow crack growth in a ceria stabilized zirconia-alumina nanocomposite for medical applications, *Biomaterials*, **29**, 3636 – 3641, (2008).

20 Kern, F.: Gadolinia-Neodymia-Co-stabilized zirconia materials with high toughness and strength, *J. Ceram. Sci. Techn.*, **3**, [3], 119 – 130, (2012).

21 Toraya, H., Yoshimura, M., Somiya, S.: Calibration curve for quantitative analysis of the monoclinic-tetragonal ZrO_2 system by X-ray diffraction, *J. Am. Ceram. Soc.*, **67**, [6], C119 – 121, (1984).

22 Kosmac, T., Wagner, R., Claussen, N.: X-ray determination of transformation depths in ceramics containing tetragonal ZrO_2, *J. Am. Ceram. Soc.*, **64**, [4], C72 – 73, (1981).

23 McMeeking, R., Evans, A.G.: Mechanics of transformation toughening in brittle materials, *J. Am. Ceram. Soc.*, **65**, [5], 242 – 246, (1982).

24 Mendelson, M.I.: Average grain size in polycrystalline ceramics, *J. Am. Ceram. Soc.*, **52,** [8], 443 – 446, (1969).

25 Lube, T., Fett, T: A threshold stress intensity factor at the onset of stable crack extension of knoop indentation cracks, *Eng. Fract. Mech.*, **71**, 2263 – 2269, (2004).

26 Gutknecht, D., Chevalier, J., Garnier, V., Fantozzi, G.: Key role of processing to avoid low temperature ageing in alumina zirconia composites for orthopaedic application, *J. Eur. Ceram. Soc.*, **27**, 1547 – 1552, (2007).

[27] Heuer, A.H., Claussen, N., Kriven, W.M., Rühle, M.: Stability of tetragonal ZrO_2 particles in ceramic matrices, *J. Am. Ceram. Soc.*, **65**, [12], 642 – 650, (1982).

[28] He, M.Y., Hutchinson, J.W.: Kinking of a crack out of an interface, *J. Appl. Mech.,* **56**, 270 – 278, (1989).

[29] Lakiza, S.M., Lopato, L.M.: Phase diagram of the Al_2O_3-ZrO_2-La_2O_3 system, *J. Eur. Ceram. Soc.*, **25**, 1373 – 1380, (2005).

[30] Wang, C., Zinkevich, M., Aldinger, F.: Phase diagrams and thermodynamics of rare-earth-doped zirconia ceramics, *Pure Appl. Chem.*, **79**, (10), 1731 – 1753, (2007).